RSC Advances

PAPER

View Article Online
View Journal | View Issue

Cite this: *RSC Adv.*, 2019, **9**, 29141

A bifunctional sensor based on diarylethene for the colorimetric recognition of Cu^{2+} and fluorescence detection of Cd^{2+}†

Shouyu Qiu, Mengmeng Lu, Shiqiang Cui, * Zhen Wang and Shouzhi Pu*

Received 2nd July 2019
Accepted 4th September 2019

DOI: 10.1039/c9ra04965g

rsc.li/rsc-advances

A novel bifunctional sensor based on diarylethene with a benzyl carbazate unit was synthesized successfully. It not only served as a colorimetric sensor for the recognition of Cu^{2+} by showing changes in absorption spectra and solution color, but also acted as a fluorescent sensor for the detection of Cd^{2+} through obvious emission intensity enhancement and fluorescence color change. The sensor exhibited excellent selectivity and sensitivity towards Cu^{2+} and Cd^{2+}, and the limits of detection for Cu^{2+} and Cd^{2+} were 8.36×10^{-8} mol L^{-1} and 1.71×10^{-7} mol L^{-1}, respectively, which were much lower than those reported by the WHO and EPA in drinking water. Furthermore, its application in practical samples demonstrated that the sensor can be effectively applied for the detection of Cu^{2+} and Cd^{2+} in practical water samples.

Introduction

Heavy metal contamination is harmful to the environment and human health and is attracting considerable attention nowadays. Among various heavy metals, copper is the third most copious trace element in human bodies and plays a critical role in a series of physiological processes.[1–4] However, abnormal levels of Cu^{2+} are detrimental to human health, not only leading to hematologic manifestations[5] and several neurodegenerative diseases, such as Wilson's disease, Menkes disease, Parkinson's disease, and Alzheimer's disease,[6–10] but also resulting in gastrointestinal disorders and damage to the liver and kidneys.[11,12] According to the regulations of the U.S. Environmental Protection Agency (EPA), the maximum acceptable concentration of copper is nearly 20 μM in drinking water.[13] The World Health Organization (WHO) has also stated the maximum allowable level of copper at 31.47 μM in drinking water.[14] On the other hand, cadmium, one of the most important heavy metal elements, has been widely used in various agricultural and industrial activities including electroplating, paint pigmentation, nickel–cadmium batteries, and chemical fertilizers,[15–17] which has resulted in the widespread distribution of Cd^{2+} in the environment. Cd^{2+} is highly toxic in nature even at very low concentrations, and the maximum permissible concentrations of cadmium ions in drinking water are regulated by the WHO and EPA to be 3 μg L^{-1} and 1.8 μg L^{-1}, respectively.[18,19] Furthermore, Cd^{2+} is not only non-biodegradable, but can also be easily absorbed and accumulated in human bodies and food chains from the environment and retained over a long period of time,[20] which causes serious damage to the human nervous system, kidneys, lungs, and many other tissues.[21–24] Therefore, it is particularly important to monitor the levels of Cu^{2+} and Cd^{2+} in environmental and biological samples.

A number of analytical methods have been utilized for the detection of heavy metal ions, such as atomic absorption spectroscopy (AAS), inductively coupled plasma mass spectrometry (ICP-MS), and electrochemical methods;[25–28] however, the expensive instruments, time-consuming operations, *in situ* analysis, and real-time environmental monitoring are the main drawbacks. Compared to the abovementioned methods, chemosensing as one of the most promising approaches has attracted more attention due to its advantages of a fast response, high sensitivity, high selectivity, and real-time analysis.[29,30] Up to now, great efforts have been devoted to develop highly selective and sensitive chemosensors for the detection of heavy metal ions. Although sensors for the colorimetric recognition of Cu^{2+} (ref. 31–36) and fluorescence detection of Cd^{2+} have been extensively reported,[37–40] some of them display low sensitivity to Cu^{2+} or Cd^{2+}. On the other hand, there are few reports on chemosensors capable of detecting copper ions by colorimetry and cadmium ions by the fluorescence method.[41] Hence, the design and synthesis of a highly sensitive and selective sensor for the colorimetric identification of Cu^{2+} and fluorescence-based identification of Cd^{2+} are still huge challenges.

Diarylethene derivatives as sensors for detecting ions have attracted considerable interest owing to their good thermal stability, excellent fatigue resistance, and high reactivity.[42–45] In

Jiangxi Key Laboratory of Organic Chemistry, Jiangxi Science and Technology Normal University, Nanchang 330013, PR China. E-mail: cuisq2006@163.com; pushouzhi@tsinghua.org.cn; Fax: +86-791-83831996; Tel: +86-791-83831996

† Electronic supplementary information (ESI) available. See DOI: 10.1039/c9ra04965g

recent years, numerous multifunctional diarylethene-based sensors have been designed and synthesized. In contrast, only a few studies about sensors based on diarylethene for the colorimetric detection of Cu^{2+} and fluorescence detection of Cd^{2+} have been reported.[41] In this work, a novel sensor for the colorimetric recognition of Cu^{2+} and fluorescence detection of Cd^{2+} based on diarylethene with a benzyl carbazate unit was successfully designed and synthesized, as displayed in Scheme 1. Meanwhile, its multifunctional switching characteristics induced by light, Cu^{2+}, and Cd^{2+} were systematically investigated in THF. The structural characterization data of **1o** including ^{1}H NMR, ^{13}C NMR, and ESI-MS are presented in supplementary information (Fig. S1–S3†).

Experimental

General methods

All the chemical reagents used in the experiments were purchased from commercial sources and were not purified further prior to use. The solutions of metal ions (0.1 mol L^{-1}) used in the tests were prepared by dissolving the corresponding metal nitrates in distilled water except for K^+, Ba^{2+}, Hg^{2+} and Sn^{2+} (their counter ions were chloride ions). The NMR spectra were measured with tetramethylsilane (TMS) as the internal standard on a Bruker AV400 spectrometer. Mass spectra were recorded with a Bruker Amazon SL ion trap mass spectrometer (ESI) using methanol as the solvent. The melting points were determined on a WRS-1B melting point apparatus. The absorption spectra and fluorescence spectra were collected on an Agilent 8454 UV/vis spectrometer and a Hitachi F-4600 fluorescence spectrophotometer, respectively. Moreover, MUA-165 UV lamp and MVL-210 visible lamp were used for photo-irradiation. The fluorescence quantum yield was determined on an Absolute PL Quantum Yield Spectrometer QYC11347-11. Infrared spectra (IR) were collected on a BrukerVertex-70 spectrometer. Unless otherwise indicated, all measurements were made at room temperature, and the sample concentration was maintained at 2.0×10^{-5} mol L^{-1}.

Synthesis of the target compound

The target compound **1o** was synthesized through a simple one-step reaction, and the synthetic route is shown in Scheme 1. First, compound **2** was synthesized according to a previously reported method.[46,47] Second, compound **2** (0.098 g, 0.2 mmol) and compound **3** (0.034 g, 0.2 mmol) were dissolved in absolute ethanol (5.0 mL) in a round-bottom flask (25 mL), followed by the addition of one drop of ethylic acid in the reaction solution. A purple precipitate was observed after the reaction system was continuously stirred for 12 h at room temperature. Then, the resulting purple precipitate was filtered, washed for 3 times with absolute ethanol and dried in vacuum to obtain **1o** as a purple solid with a yield of 57% (0.072 g). Mp: 450–452 K. ^{1}H NMR (400 MHz, DMSO-d_6, TMS), δ (ppm): 1.83 (s, 3H), 1.92 (s, 3H), 2.38 (s, 3H), 5.18 (s, 2H), 6.82 (s, 1H), 7.42–7.30 (m, 5H), 7.68 (s, 1H), 7.86 (d, 1H, $J = 8.0$ Hz), 8.04 (s, 1H), 8.09 (d, 1H, $J = 8.0$ Hz), 8.84 (s, 1H), 11.57 (s, 1H). ^{13}C NMR (100 MHz, DMSO-d_6, TMS), δ (ppm): 14.4, 14.5, 15.1, 66.7, 116.3, 120.2, 123.9, 124.8, 124.9, 126.0, 128.5, 128.6, 128.9, 129.1, 130.1, 133.6, 136.9, 138.1, 138.7, 140.3, 142.9, 144.6, 146.2, 152.9, 153.7. IR (KBr, ν, cm^{-1}): 3551, 3484, 3413, 2963, 2923, 2856, 1752, 1603, 1548, 1497, 1444, 1378, 1345, 1262, 1222, 1106, 1053. ESI-MS: m/z = 636.0, $[M + H^+]^+$ calcd 636.1.

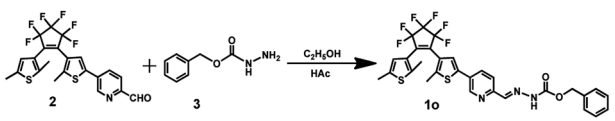

Scheme 1 The synthetic route and photochromism of **1o**.

Results and discussion

Photochromic properties of 1o

The photochromic properties of **1o** were investigated upon irradiation with UV/vis in a THF solution (2.0×10^{-5} mol L^{-1}) at room temperature. As shown in Fig. S4,† **1o** shows a sharp absorption peak at 336 nm ($\varepsilon = 4.2 \times 10^4$ mol^{-1} L cm^{-1}), which can be attributed to the π–π* transition.[48] Upon irradiation with a 365 nm light, the absorption peak at 336 nm decreased gradually, while a new absorption band centered at 563 nm ($\varepsilon = 1.1 \times 10^4$ mol^{-1} L cm^{-1}) appeared and increased gradually due to the formation of the closed-ring isomer **1c** with increased π–electron delocalization in the molecule.[49,50] The color of the solution changed from colorless to purple simultaneously. After irradiating with a 365 nm light for 2 min, the photostationary state (PSS) was reached, and an obvious isosbestic point was observed at 355 nm, indicating that photochromism is a two-component reaction.[51–53] Contrarily, upon irradiation with visible light (λ > 500 nm) for 2.0 min, the color of the solution of **1c** changed from purple to colorless, indicating that the ring-closed isomer **1c** underwent a cycloreversion reaction and returned to the initial ring-open isomer **1o** structure.[54,55] The quantum yields of the cyclization and cycloreversion reactions of **1o** were determined to be 0.30 and 0.03, respectively, with 1,2-bis(2-methyl-5-phenyl-3-thienyl)perfluorocyclopentene as a ref. 56.

Colorimetric sensing of Cu^{2+} by 1o

The colorimetric properties of **1o** towards metal ions including Cu^{2+}, Sn^{2+}, Ca^{2+}, K^+, Ag^+, Ni^{2+}, Ba^{2+}, Mg^{2+}, Mn^{2+}, Cd^{2+}, Sr^{2+}, Hg^{2+}, Co^{2+}, Cr^{3+}, Fe^{3+}, Pb^{2+}, Zn^{2+}, and Al^{3+} were investigated in THF. As shown in Fig. 1, upon the addition of 1.0 equiv. of various metal ions, although the absorption at 336 nm shows different changes, only Cu^{2+} and Ni^{2+} induced the appearance of new absorption peaks at 413 nm. Meanwhile, the colors of the solutions changed immediately from colorless to yellow and pale yellow with the addition of Cu^{2+} and Ni^{2+}, respectively. Compared to the color of the solution with Cu^{2+}, the color of the solution with Ni^{2+} was negligible. Additionally, in order to explore the practical application of **1o** in Cu^{2+} detection, competitive experiments were carried out in the presence of Cu^{2+} mixed with the other metal ions mentioned above. As shown in Fig. S5,† upon the addition of 1.0 equiv. of Cu^{2+}, the coexistent metal ions, even Ni^{2+}, hardly affect the determination

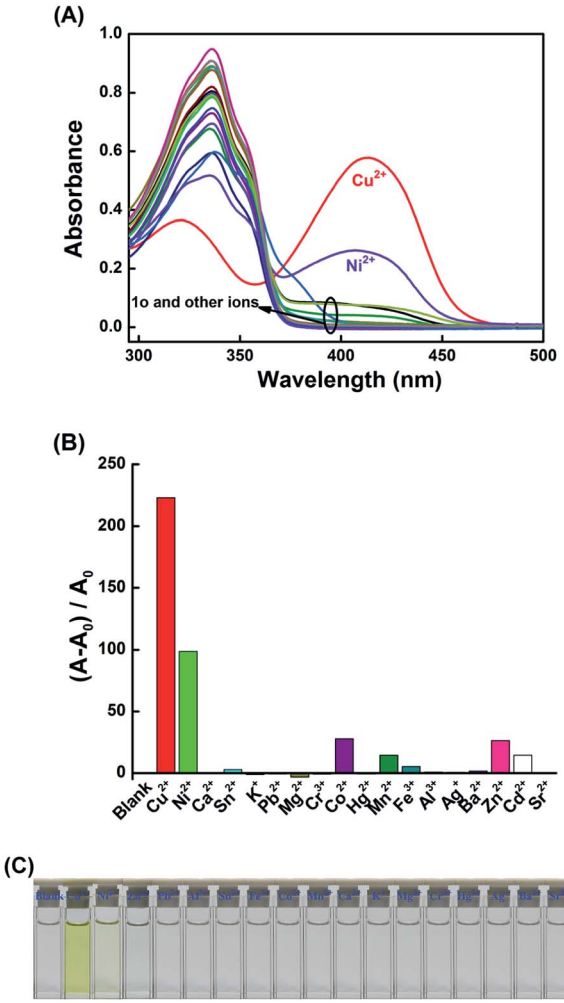

Fig. 1 Changes in the absorption of **1o** (2.0×10^{-5} mol L^{-1}) induced by various metal ions (1.0 equiv.) in THF: (A) UV-vis absorption spectral changes; (B) absorbance at 413 nm in the presence of different metal ions; (C) photo demonstrating the colors of the **1o** solutions containing different metal ions.

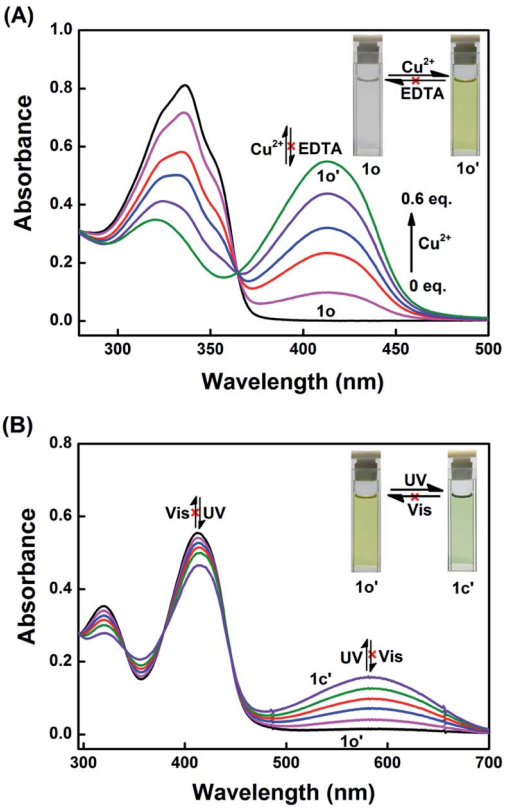

Fig. 2 Absorption spectra and color changes of **1o** (A) in THF (2.0×10^{-5} mol L^{-1}) with the addition of Cu^{2+} ion, and (B) **1o′** upon irradiation with UV/vis lights.

of Cu^{2+} by **1o** in THF. These results suggested that **1o** could act as a potential colorimetric sensor of Cu^{2+} in practical samples.

UV-vis titration experiments were performed to investigate the binding mode between **1o** and Cu^{2+}. As depicted in Fig. 2A, upon the gradual addition of Cu^{2+} to the solution of **1o**, the absorption at 336 nm decreases and a blue shift is observed from 336 nm to 320 nm. At the same time, a new absorption band centered at 413 nm emerged and increased gradually, which might be ascribed to the metal-to-ligand charge transfer (MLCT),[57] resulting in a color change of the solution from colorless to yellow. After 0.6 equiv. of Cu^{2+} was added, the absorbance intensity at 413 nm reached saturation and remained unchanged with further titration (Fig. S6†). An isosbestic point was observed at 365 nm, indicating that only one stable complex **1o**-Cu^{2+} (**1o′**) was formed between **1o** and Cu^{2+}. However, the absorption spectrum of **1o** could not be recovered when excessive EDTA was added.

The photochromism of **1o′** was also investigated by alternating the irradiation between UV and visible lights. As shown in Fig. 2B, upon irradiation with 365 nm light, the absorptions at 320 nm and 413 nm decreased gradually, and two new absorption bands at 356 nm and 584 nm emerged and increased simultaneously. In accordance with the change in the absorption spectrum, the color of the solution changed from yellow to olive due to the formation of the closed-ring isomer **1c**-Cu^{2+} complex (**1c′**). After irradiation for 3.0 minutes, PPS was achieved, and three isosbestic points were observed at 342 nm, 379 nm, and 442 nm. However, the absorption spectrum of **1o′** could not be completely recovered upon irradiation with visible light ($\lambda > 500$ nm). When Cu^{2+} was gradually added to the solution of **1c**, the absorption band centered at 340 nm decreased distinctly, and a new absorption band centered at 420 nm appeared and increased. At the same time, the absorption peak at 563 nm increased slightly and red-shifted to 584 nm, accompanied by the color change of the solution from purple to olive (Fig. S7†). A well-defined isosbestic point was observed at 376 nm, revealing the formation of the complex **1c′**. When excess EDTA was added, the absorption spectrum could not recover to that of **1c**.

Fluorescence response of 1o to Cd^{2+}

The fluorescence responses of **1o** to various metal ions including Cu^{2+}, Sn^{2+}, Ca^{2+}, K^{+}, Ag^{+}, Ni^{2+}, Ba^{2+}, Mg^{2+}, Mn^{2+}, Cd^{2+}, Sr^{2+}, Hg^{2+}, Co^{2+}, Cr^{3+}, Fe^{3+}, Pb^{2+}, Zn^{2+}, and Al^{3+} were also investigated in THF. As shown in Fig. 3A, **1o** displays very weak fluorescence with 340 nm light excitation, and the quantum

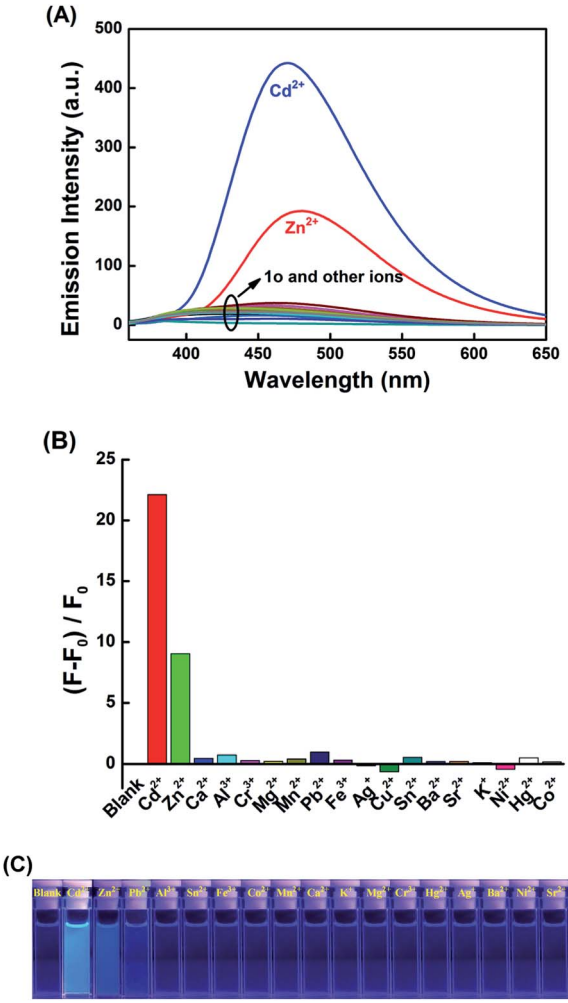

Fig. 3 Changes in the fluorescence of **1o** (2.0×10^{-5} mol L^{-1}) induced by various metal ions (4.0 equiv.) in THF: (A) fluorescence emission spectral changes (λ_{ex} = 340 nm); (B) emission intensity changes; (C) color changes (under 365 nm light).

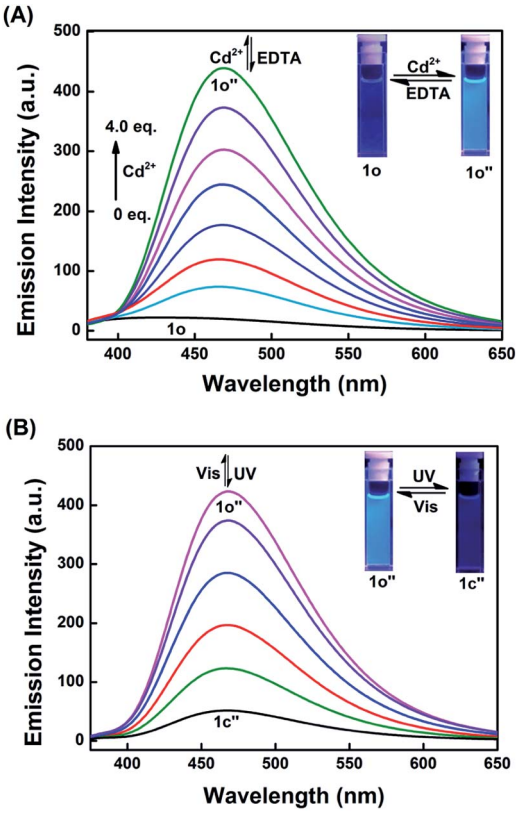

Fig. 4 Fluorescence spectral changes and color responses of (A) **1o** in THF (2.0×10^{-5} mol L^{-1}) induced by Cd^{2+} (0–4.0 equiv.) and (B) **1o**″upon irradiation with UV and visible lights (λ_{ex} = 340 nm).

yield is determined to be 0.002. Upon the addition of 4.0 equiv. of metal ions, only Cd^{2+} induced prominent fluorescence enhancement at 470 nm, while the other metal ions did not show any significant effects (Fig. 3B). It was noteworthy that Zn^{2+} could also cause fluorescence enhancement, but the enhancement could be ignored compared to that of Cd^{2+}. Under the 365 nm light, the changes in the fluorescence color of **1o** induced by various metal ions were recorded, and only Cd^{2+} induced an obvious color change that could be seen by the naked eyes (Fig. 3C). These results indicated that **1o** can act as a fluorescent sensor for the detection of Cd^{2+}. Competitive experiments were also carried out by adding 4.0 equiv. of Cd^{2+} to the solutions containing **1o** and various metal ions (4.0 equiv. of **1o**). As shown in Fig. S8,† the coexistence of ions hardly interferes with the detection of cadmium ions except for Ni^{2+} and Sn^{2+}. It is noteworthy that Cu^{2+} could significantly quench the fluorescence of **1o**-Cd^{2+}, which may be due to its paramagnetism.[58]

The fluorescence titration of **1o** with Cd^{2+} was performed in THF at room temperature. As shown in Fig. 4A, upon the gradual addition of 0 to 4.0 equiv. Cd^{2+} to the solution of **1o**, the emission intensity of **1o** increased gradually and reached saturation (Fig. S9†). At the end of titration, the emission intensity enhanced 22-fold, with the emission peak shifting from 430 nm to 470 nm, which was ascribed to the formation of a new complex **1o**-Cd^{2+} (**1o**″). With further titration, the fluorescence intensity remained unchanged. The fluorescence color changed from dark to bright blue, and the fluorescence quantum yield of **1o**″ was determined to be 0.01. The weak fluorescence of **1o** was attributed to the isomerization of the C=N bond.[39,59] After the addition of Cd^{2+}, a stable complex **1o**″ was formed, which inhibited the isomerization of the C=N bond and increased the rigidity of the molecule, resulting in a chelation enhanced fluorescence (CHEF) effect.[60,61] The fluorescence spectrum of **1o** could be recovered by adding 60 equiv. of EDTA, indicating that the complexation/decomplexation between **1o** and Cd^{2+} was reversible.

The **1o**″ complex also exhibited excellent fluorescence switching properties. As shown in Fig. 4B, upon irradiation with 365 nm light, the emission intensity of **1o**″ at 470 nm is quenched by 88% at PPS, indicating that **1o**″ exhibits relatively high fluorescence modulation efficiency. The decrease in the emission intensity was attributed to the formation of the closed-ring isomer **1c**-Cd^{2+} complex (**1o**″),[62] and the fluorescence resonant energy transfer (FRET) process occurred.[63,64] The fluorescence spectrum of **1o**″ could be recovered upon irradiation with visible light (λ > 500 nm). The fluorescence titration experiments

of **1c** with Cd^{2+} were also carried out in THF. Upon the addition of 4.0 equiv. of Cd^{2+} to the solution of **1c**, the fluorescence intensity at 470 nm increased by 4-fold due to the formation of **1o″** (Fig. S10†). Similarly, the fluorescence spectrum of **1c** could be recovered by adding 60 equiv. of EDTA, indicating that the complexation between **1c** and Cd^{2+} was also reversible.

Complexation mechanism of 1o with Cu^{2+} and Cd^{2+}

The stoichiometry between **1o** and Cu^{2+}/Cd^{2+} was determined by Job's plot analysis.[65] As shown in Fig. 5A, the maximum absorbance appears at the molar ratio of 0.5, indicating that the binding mode between **1o** and Cu^{2+} is 1 : 1. The mass spectrum peak at $m/z = 820.8$ corresponding to $[\mathbf{1o} + Cu^{2+} + 2NO_3^- - H^+]^-$ (calcd: 821.0) further confirmed the 1 : 1 stoichiometry (Fig. S11†). On the basis of the 1 : 1 binding mode between **1o** and Cu^{2+}, the association constant (K_a) was calculated to be 1.25×10^4 L mol^{-1} ($R = 0.994$) (Fig. 5B), and the limit of detection (LOD) of **1o** towards Cu^{2+} was calculated to be 8.36×10^{-8} mol L^{-1} based on $3\delta/s$ (ref. 66 and 67) (Fig. S12†). Similarly, the Job's plot also indicated the formation of a 1 : 1 complex between **1o** and Cd^{2+}(Fig. 6A). Additionally, ESI-MS was performed for further verifying the binding stoichiometry; a signal peak at $m/z = 871.7$ was assigned to $[\mathbf{1o} + Cd^{2+} + 2NO_3^- - H^+]^-$ (calcd: 871.9) (Fig. S13†), which was consistent with the stoichiometry of 1 : 1. Based on the 1 : 1 binding mode, the

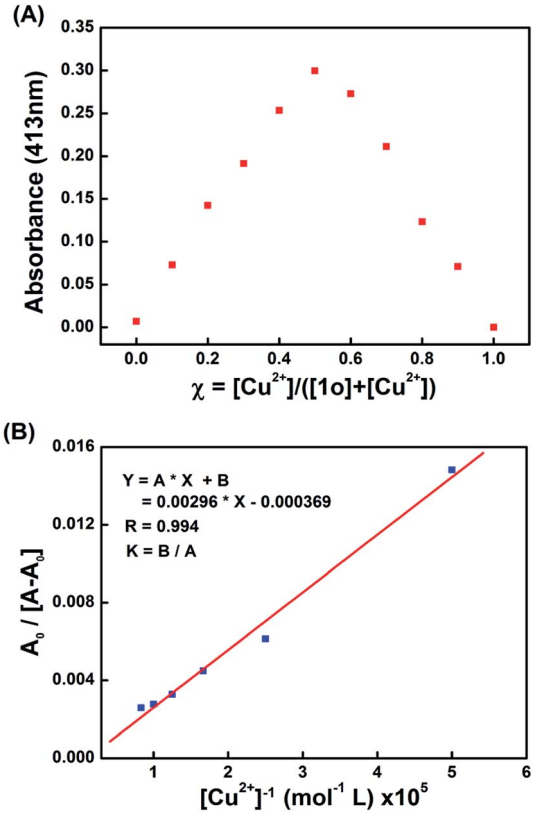

Fig. 5 (A) Job's plot showing the 1 : 1 complex of **1o** and Cu^{2+}, and (B) Benesi–Hildebrand plot based on the 1 : 1 binding stoichiometry. The binding constant of **1o** with Cu^{2+} was calculated to be 1.25×10^4 L mol^{-1}.

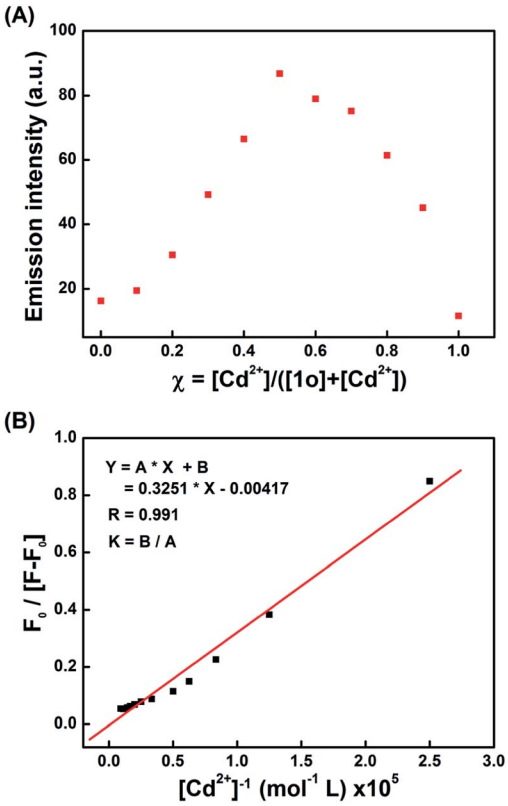

Fig. 6 Job's plot showing the 1 : 1 complex of **1o** and Cd^{2+} (A) and (B) Benesi–Hildebrand plot based on the 1 : 1 binding stoichiometry; the binding constant of **1o** with Cd^{2+} was calculated to be 1.28×10^3 L mol^{-1}.

association constant (K_a) was calculated to be 1.28×10^3 L mol^{-1} ($R = 0.991$) (Fig. 6B). The detection limit of **1o** towards Cd^{2+} was determined to be 1.71×10^{-7} mol L^{-1} (Fig. S14†). The detection limit of **1o** was much lower than those of the reported sensors for Cu^{2+} or Cd^{2+} (Table S1†).[32,41,68–74] The results displayed that **1o** not only acted as a colorimetric sensor for Cu^{2+}, but also served as a fluorescent sensor for Cd^{2+} with high sensitivity.

^{1}H NMR titration and IR spectral results were recorded to further explore the interaction between **1o** and Cu^{2+}/Cd^{2+}. First, the binding mode between **1o** and Cu^{2+} was investigated, and the ^{1}H NMR titration did not provide useful information due to the paramagnetic nature of Cu^{2+}.[57] In the IR spectrum of **1o**, the stretching vibration absorption peaks at 1603, 1548, 1497, and 1444 cm^{-1} are assigned to the pyridine unit; the absorption peaks at 1752 and 1617 cm^{-1} are assigned to the stretching vibrations of C=O and C=N, respectively (Fig. S15†). When Cu^{2+} was added, the stretching vibration peaks of the pyridine unit remained almost unaffected, indicating that the N atom of the pyridine unit did not participate in the coordination process. It could be clearly seen that the absorption peaks at 1617 and 1752 cm^{-1} shifted severally to 1657 and 1725 cm^{-1}, suggesting that the N atom of the Schiff base unit and the O atom in C=O are more likely the binding sites for Cu^{2+} coordination. Then, the interacting mode between **1o** and Cd^{2+} was further investigated. As depicted in Fig. 7, with the addition of

Cd^{2+}, the signals (H_b, H_c, H_d) assigned to the pyridine ring and Schiff base displayed downfield shifts from 8.77, 8.02 and 7.97 ppm to 8.85, 8.27 and 8.17 ppm, respectively. However, the signal (H_e) at 7.97 ppm exhibited an upfield shift to 7.77 ppm. These shifts may be attributed to the coordinate bond between Cd^{2+} and the N atom on the pyridine unit or the Schiff base unit. Notably, the signal at 5.20 ppm ascribed to methylene displayed a 0.13 ppm downfield shift to 5.36 ppm, and the proton signal at 10.45 ppm (H_a) assigned to –NH had a large downfield shift to 12.14 ppm, which may be caused by the isomerization of the amide unit (NH–C=O) and the formation of a new N=C–OH structure. The coordination of the O atom with Cd^{2+} led to the decrease in the electron cloud density of the O atom and resulted in a large downfield shift of the proton signal (Ha).[75] In the IR spectra, upon the addition of Cd^{2+}, the stretching vibration absorption peaks of the pyridine unit changed slightly, while it could be seen that the absorption peak of C=N at 1617 cm^{-1} shifted to 1649 cm^{-1}. The results further confirmed that the N atoms of the Schiff base unit were involved in coordination with Cd^{2+}. It was worth noting that the peak at 1752 cm^{-1} assigned to C=O disappeared, and a new absorption peak appeared at 1694 cm^{-1}, indicating that the isomerization of the amide unit (NH–C=O) occurred and resulted in the formation of a new N=C–OH structure. The results further confirmed that the N atom of the Schiff base unit and the O atom of the N=C–OH unit participated in coordination. The appearance of absorption peaks at 2397 and 2428 cm^{-1} was attributed to the formation of the large conjugated system (C=N–N=C) (Fig. S15†). Therefore, in the ^1H NMR titration, the changes in signals (H_a, H_f) were ascribed to the isomerization of amides. Based on these results, a reasonable binding mode between **1o** and Cu^{2+}/Cd^{2+} is exhibited in Scheme 2, and the optimized structures of **1o**-Cu^{2+} and **1o**-Cd^{2+} are shown in Fig. S16.†

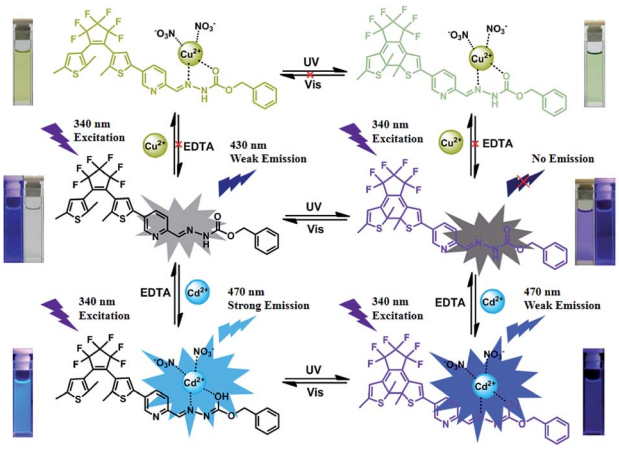

Scheme 2 Changes in the photochromism, color and absorption of **1o** induced by Cu^{2+}/EDTA and UV-vis lights, and the multi-controlled fluorescence-switching behaviors of **1o** induced by UV/vis lights and Cd^{2+}/EDTA.

Application in real water samples

To further explore the potential application of the sensor **1o** in actual water samples, real samples including those obtained from the Ganjiang River and tap water were collected from Nanchang City and analyzed according to the methods reported previously.[76,77] For better results and analysis of Cu^{2+} and Cd^{2+} in the water samples, the collected water samples were pretreated with a 0.2 μm membrane to remove suspended substances; then, different amounts of Cu^{2+} and Cd^{2+} were spiked separately into the real water samples to evaluate their recovery. The recoveries of Cu^{2+} and Cd^{2+} added in the real samples were calculated, and the results are summed up in Tables 1 and 2, respectively. It could be seen that the recoveries for Cu^{2+} ranged from 98.0% to 104.7%, while those for Cd^{2+} ranged between 97.2% and 103.9%, revealing the high accuracy of the sensor **1o** and its potential applications for the determination of Cu^{2+} and Cd^{2+} in practical water samples.

Table 1 Application in practical samples for the detection of Cu^{2+}

Sample	Cu^{2+} added (μmol L^{-1})	Cu^{2+} determined (μmol L^{-1})	Recovery (%)
Ganjiang River	4	4.10	102.5
	6	6.28	104.7
	8	7.96	99.5
	10	10.35	103.5
Tap water	4	3.92	98.0
	6	6.08	101.3
	8	7.89	98.6
	10	10.08	100.8

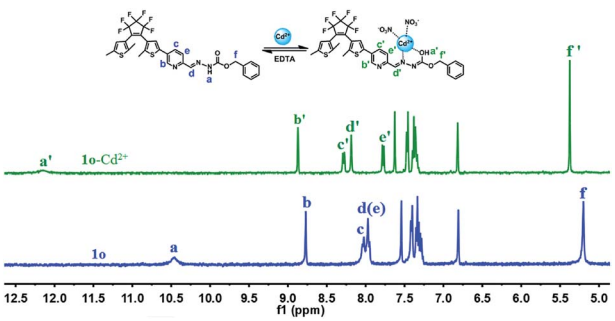

Fig. 7 ^1H NMR spectra of **1o** and **1o**-Cd^{2+} in THF-d_8 (inset shows the proposed binding mode of the complex **1o**″).

Table 2 Application in practical samples for the detection of Cd^{2+}

Sample	Cd^{2+} added (μmol L^{-1})	Cd^{2+} determined (μmol L^{-1})	Recovery (%)
Ganjiang River	4	4.08	102.0
	8	7.77	97.2
	12	11.80	98.3
	16	16.07	100.4
Tap water	4	4.06	101.5
	8	8.31	103.9
	12	12.34	102.8
	16	15.91	99.4

Conclusions

In summary, a novel bifunctional sensor for the colorimetric detection of Cu^{2+} and fluorescence detection of Cd^{2+} based on diarylethene with a benzyl carbazate unit was synthesized successfully. The detection limits for Cu^{2+} and Cd^{2+} were 8.36×10^{-8} mol L^{-1} and 1.71×10^{-7} mol L^{-1}, respectively, which were much lower than the values allowed by the WHO and EPA in drinking water. The results from the applications in real samples indicated that the sensor could be used to detect Cu^{2+} and Cd^{2+} in practical samples with high accuracy. The results will provide us a new thought for the design and synthesis of multi-functional sensors.

Conflicts of interest

There are no conflicts of interest to declare.

Acknowledgements

The authors are grateful for the financial support from the National Natural Science Foundation of China (41867053), the "5511" Science and Technology Innovation Talent project of Jiangxi (2016BCB18015), the key project of Natural Science Foundation of Jiangxi Province (20171ACB20025), the Young Talents Project of Jiangxi Science and Technology Normal University (2015QNBJRC004), and the Master Graduate Innovation Special Foundation of Jiangxi Province (YC2018-S407).

Notes and references

1 P. Milindanuth and P. Pisitsak, *Mater. Chem. Phys.*, 2018, **216**, 325–331.
2 R. Martínez, A. Espinosa, A. Tárraga and P. Molina, *Tetrahedron*, 2008, **64**, 2184–2191.
3 Y. Guo, Z. Wang, W. Qu, H. Shao and X. Jiang, *Biosens. Bioelectron.*, 2011, **26**, 4064–4069.
4 J. Fan, P. Zhan, M. Hu, W. Sun, J. Tang, J. Wang, S. Sun, F. Song and X. Peng, *Org. Lett.*, 2013, **15**, 492–495.
5 T. R. Halfdanarson, N. Kumar, C. Y. Li, R. L. Phyliky and W. J. Hogan, *Eur. J. Haematol.*, 2008, **80**, 523–531.
6 Y. Zhou, J. Zhang, H. Zhou, Q. Zhang, T. Ma and J. Niu, *J. Lumin.*, 2012, **132**, 1837–1841.
7 L. M. Gaetke and C. K. Chow, *Toxicology*, 2003, **189**, 147–163.
8 J. S. Bains and C. A. Shaw, *Brain Res. Rev.*, 1997, **25**, 335–358.
9 G. J. Brewer, *Am. J. Clin. Nutr.*, 1998, **67**, 1087S–1090S.
10 D. G. Barceloux, *J. Toxicol., Clin. Toxicol.*, 1999, **37**, 217–230.
11 N. Kumar, *Mayo Clin. Proc.*, 2006, **81**, 1371–1384.
12 B. Sarkar, *Metal Ions in Biological Systems*, ed. H. Sigel, Marcel Dekker, New York, 1981, vol. 12, pp. 233–281.
13 J. Liu and Y. Lu, *J. Am. Chem. Soc.*, 2007, **129**, 9838–9839.
14 G. R. You, G. J. Park, J. J. Lee and C. Kim, *Dalton Trans.*, 2015, **44**, 9120–9129.
15 F. Beck and P. Rüetschi, *Electrochim. Acta*, 2000, **45**, 2467–2482.
16 C. L. Han, L. H. Wu, W. N. Tan, D. X. Zhong, Y. J. Huang, Y. M. Luo and P. Christie, *Environ. Geochem. Health*, 2012, **34**, 481–492.
17 R. L. Chaney, J. A. Ryan, Y. M. Li and S. L. Brown, *Soil Cadmium as a Threat to Human Health, Cadmium in Soils and Plants*, Springer Netherlands, 1999, pp. 219–256.
18 World Health Organization (WHO), *Guidelines for Drinking-Water Quality*, World Health Organization, Geneva, 4th edn, 2011, p. 327.
19 USA Environmental Protection Agency, *Aquatic Life, Ambient Water QualityCriteria, Cadmium-2016, EPA 820-R-16-002*, Office of Water, Office of Science and Technology, Health and Ecological Criteria Division, Washington D.C., USA, 2016 March.
20 Y. Li, T. Xia, J. Zhang, Y. Cui, B. Li, Y. Yang and G. Qian, *J. Solid State Chem.*, 2019, **275**, 38–42.
21 A. Åkesson, B. Julin and A. Wolk, *Cancer Res.*, 2008, **68**, 6435–6441.
22 J. A. McElroy, M. M. Shafer, A. T. Dietz, J. M. Hampton and P. A. Newcomb, *J. Natl. Cancer Inst.*, 2006, **98**, 869–873.
23 M. P. Waalkes, *J. Inorg. Biochem.*, 2000, **79**, 241–244.
24 M. Waisberg, P. Joseph, B. Hale and D. Beyersmann, *Toxicology*, 2003, **192**, 95–117.
25 S. M. Z. Hossain and J. D. Brennan, *Anal. Chem.*, 2011, **83**, 8772–8778.
26 A. Lafaye, C. Junot, B. R. L. Gall, P. Fritsch, J. C. Tabet and E. Ezan, *Rapid Commun. Mass Spectrom.*, 2003, **17**, 2541–2549.
27 C. Liu, S. He, K. Shen, X. Feng, G. Fang and S. Wang, *Food Anal. Methods*, 2015, **8**, 1785–1793.
28 N. Li, D. Zhang, Q. Zhang, Y. Lu, J. Jiang, G. L. Liu and Q. Liu, *Sens. Actuators, B*, 2016, **231**, 349–356.
29 R. V. Rathod, S. Bera, M. Singh and D. Mondal, *RSC Adv.*, 2016, **6**, 34608–34615.
30 L. Yan, R. Li, F. Ma and Z. Qi, *Anal. Methods*, 2017, **9**, 1119–1124.
31 N. Chakraborty, A. Chakraborty and S. Das, *J. Lumin.*, 2018, **199**, 302–309.
32 Q. Huang, Y. T. Chen, Y. W. Ren, Z. Y. Wang, Y. X. Zhu and Y. Zhang, *Anal. Methods*, 2018, **10**, 5731–5737.
33 P. Sengupta, A. Ganguly and A. Bose, *Spectrochim. Acta, Part A*, 2018, **198**, 204–211.
34 L. Wang, Q. Bing, J. Li and G. Wang, *J. Photochem. Photobiol., A*, 2018, **360**, 86–94.
35 L. Zhang, R. Wang, R. Liu, X. Du, R. Meng, L. Liu and J. Yao, *Cellulose*, 2018, **25**, 6947–6961.
36 S. Guo, G. Liu, C. Fan and S. Pu, *Sens. Actuators, B*, 2018, **266**, 603–613.
37 Y. Pan, J. Wang, X. Guo, X. Liu, X. Tang and H. Zhang, *J. Colloid Interface Sci.*, 2018, **513**, 418–426.
38 Z. Wang, S. Cui, S. Qiu and S. Pu, *Tetrahedron*, 2018, **74**, 7431–7437.
39 X. Zhang, R. Wang, C. Fan, G. Liu and S. Pu, *Dyes Pigm.*, 2017, **139**, 208–217.
40 Z. Wang, S. Cui, S. Qiu and S. Pu, *J. Photochem. Photobiol., A*, 2018, **367**, 212–218.

41 H. L. Liu, S. Q. Cui, F. Shi and S. Z. Pu, *Dyes Pigm.*, 2019, **161**, 34–43.
42 S. Kawai, T. Nakashima, K. Atsumi, T. Sakai, M. Harigai, Y. Imamoto and T. Kawai, *Chem. Mater.*, 2007, **19**, 3479–3483.
43 X. Li and H. Tian, *Tetrahedron Lett.*, 2005, **46**, 5409–5412.
44 H. Samachetty and N. Branda, *Pure Appl. Chem.*, 2006, **78**, 2351–2359.
45 Q. Luo, H. Cheng and H. Tian, *Polym. Chem.*, 2011, **2**, 2435–2443.
46 P. Ren, R. Wang, S. Pu, G. Liu and C. Fan, *J. Phys. Org. Chem.*, 2014, **27**, 183–190.
47 W. D. Gao, H. Li and S. Z. Pu, *J. Photochem. Photobiol., A*, 2018, **364**, 208–218.
48 S. Z. Pu, G. Liu, L. Shen and J. K. Xu, *Org. Lett.*, 2007, **9**, 2139–2142.
49 G. Liu, S. Z. Pu and X. M. Wang, *J. Photochem. Photobiol., A*, 2010, **214**, 230–240.
50 T. Nakashima, K. Miyamura, T. Sakai and T. Kawai, *Chem. - Eur. J.*, 2009, **15**, 1977–1984.
51 S. Q. Cui, S. Z. Pu and G. Liu, *Spectrochim. Acta, Part A*, 2014, **132**, 339–344.
52 H. C. Ding, G. Liu and S. Z. Pu, *Dyes Pigm.*, 2014, **103**, 82–88.
53 H. Zhang, X. X. Kou, Q. Zhang, D. H. Qu and H. Tian, *Org. Biomol. Chem.*, 2011, **9**, 4051–4056.
54 F. Hu, M. Cao, X. Ma, S. H. Liu and J. Yin, *J. Org. Chem.*, 2015, **80**, 7830–7835.
55 Z. Li, Y. Wang, M. Li, H. Zhang, H. Guo, H. Ya and J. Yin, *Org. Biomol. Chem.*, 2018, **16**, 6988–6997.
56 M. Irie, T. Lifka, S. Kobatake and N. Kato, *J. Am. Chem. Soc.*, 2000, **122**, 4871–4876.
57 S. Q. Cui, S. Z. Pu and Y. F. Dai, *Anal. Methods*, 2015, **7**, 3593–3599.
58 R. J. Wang, L. Diao, Q. Ren, G. Liu and S. Z. Pu, *ACS Omega*, 2019, **4**, 309–319.
59 W. K. Dong, X. L. Li, L. Wang, Y. Zhang and Y. J. Ding, *Sens. Actuators, B*, 2016, **229**, 370–378.
60 S. Patil, R. Patil, U. Fegade, B. Bondhopadhyay, U. Pete, S. K. Sahoo, N. Singh, A. Basu, R. Bendre and A. Kuwar, *Photochem. Photobiol. Sci.*, 2015, **14**, 439–443.
61 S. Patil, U. Fegade, S. K. Sahoo, A. Singh, J. Marek, N. Singh, R. Bendre and A. Kuwar, *ChemPhysChem*, 2014, **15**, 2230–2235.
62 Y. M. Xue, R. J. Wang and C. H. Zheng, *Tetrahedron Lett.*, 2016, **57**, 1877–1881.
63 S. Z. Pu, L. L. Ma, G. Liu, H. C. Ding and B. Chen, *Dyes Pigm.*, 2015, **113**, 70–77.
64 M. Bossi, V. Belov, S. Polyakova and S. W. Hell, *Angew. Chem., Int. Ed.*, 2006, **45**, 7462–7465.
65 P. Job, *Ann. Chim.*, 1928, **9**, 113–203.
66 M. Shortreed, R. Kopelman, M. Kuhn and B. Hoyland, *Anal. Chem.*, 1996, **68**, 1414–1418.
67 W. Lin, L. Yuan, Z. Cao, Y. Feng and L. Long, *Chem. - Eur. J.*, 2009, **15**, 5096–5103.
68 C. H. Min, S. Na, J. E. Shin, J. K. Kim, T. G. Jo and C. Kim, *New J. Chem.*, 2017, **41**, 3991–3999.
69 G. R. You, H. J. Jang, T. G. Jo and C. Kim, *RSC Adv.*, 2016, **6**, 74400–74408.
70 G. R. You, G. J. Park, J. J. Lee and C. Kim, *Dalton Trans.*, 2015, **44**, 9120–9129.
71 X. J. Jiang, M. Li, H. L. Lu, L. H. Xu, H. Xu and S. Q. Zang, *Inorg. Chem.*, 2014, **53**, 12665–12667.
72 G. Li, D. Zhang, G. Liu and S. Z. Pu, *Tetrahedron Lett.*, 2016, **57**, 5205–5210.
73 Z. Xu, G. Li, Y. Y. Ren, H. Huang, X. Wen, Q. Xu and L. Xu, *Dalton Trans.*, 2016, **45**, 12087–12093.
74 R. Khani, E. Ghiamati, R. Boroujerdi, A. Rezaeifard and M. H. Zaryabi, *Spectrochim. Acta, Part A*, 2016, **163**, 120–126.
75 A. Dhara, N. Guchhait, I. Mukherjee, A. Mukherjee and S. C. Bhattacharya, *RSC Adv.*, 2016, **6**, 105930–105939.
76 Y. T. Chen, Y. S. Mi and Q. F. Xie, *Anal. Methods*, 2013, **5**, 4818–4823.
77 X. Wu, J. Chen and J. X. Zhao, *Analyst*, 2013, **138**, 5281–5287.